Research Square

Preprints are preliminary reports that have not undergone peer review.
They should not be considered conclusive, used to inform clinical practice,
or referenced by the media as validated information.

Elucidating the Molecular Binding Mechanism of Banxia Xiexin Decoction Components with Acute Gastroenteritis Targets: An Integrated Approach Combining Network Pharmacology and 100-ns Molecular Dynamics Simulations

Tao Li
Hunan University of Chinese Medicine
Yuan Chen
Hunan University of Chinese Medicine
Ying Qian Zhou
Hunan University of Chinese Medicine
Li xin Du
Hunan University of Chinese Medicine
Long Zou
002161@hnucm.edu.cn
Hunan University of Chinese Medicine

Research Article

Keywords: Banxia Xiexin Decoction (BXD), acute gastroenteritis(AGE), network pharmacology, molecular docking, molecular dynamics simulation, MM-PBSA

Posted Date: March 4th, 2026

DOI: https://doi.org/10.21203/rs.3.rs-8924942/v1

License: This work is licensed under a Creative Commons Attribution 4.0 International License.
Read Full License

Additional Declarations:
No competing interests reported.

Author Contributions

Tao Li: Investigation, Data curation, Formal analysis, Writing – Original draft
Yuan Chen: Methodology, Validation
Yingqian Zhou: Visualization, Software
Lixin Du: Resources, Project administration
Long Zou: Conceptualization, Supervision, Writing – Review & Editing

All authors have read and approved the final manuscript.

Elucidating the Molecular Binding Mechanism of Banxia Xiexin Decoction Components with Acute Gastroenteritis Targets: An Integrated Approach Combining Network Pharmacology and 100-ns Molecular Dynamics Simulations

Tao Li[1], Yuan Chen[1], Ying Qian Zhou[1],Li Xin Du[1],Long Zou[1]▲

（[1]·School of Pharmacy, Hunan University of Chinese Medicine, Changsha 410208, China）

E-mail: 202004010121@stu.hnucm.edu.cn, 18230601063@163.com, 13973352931@163.com, 20223723@stu.hnucm.edu.cn, 002161@hnucm.edu.cn▲

Corresponding author: Long Zou

[Abstract]：

Objective:

This study aimed to elucidate the molecular binding mechanism and structural stability of the active components of Banxia Xiexin Decoction (BXD) against core therapeutic targets of acute gastroenteritis (AGE) using an integrated computational framework.

Methods:

Active chemical constituents and AGE-related targets were retrieved from public databases (TCMSP, SwissTargetPrediction, GeneCards). Following the construction of a protein–protein interaction (PPI) network to identify core targets, molecular docking was performed to screen key active compounds. Crucially, to validate the thermodynamic stability of ligand-target interactions, 100-ns molecular dynamics (MD) simulations were conducted using GROMACS. MM-PBSA free energy calculations and Free Energy Landscape (FEL) analyses were subsequently performed to quantify binding energetics and conformational stability.

Results:

Network analysis identified TNF and STAT3 as core targets regulated by BXD. Molecular docking revealed that isorhamnetin and 7-methoxy-2-methyl-isoflavone exhibit strong binding affinities (-8.4 and -8.7 kcal/mol, respectively) to these targets. MD simulations confirmed that the ligand-protein complexes maintained stable conformations with minimal RMSD fluctuations. Notably, MM-PBSA decomposition demonstrated a robust binding free energy of -133.97 ± 12.83 kJ/mol for the TNF–isorhamnetin complex, driven primarily by van der Waals and electrostatic interactions. FEL analysis further verified that the complexes reside in stable low-energy basins.

Conclusion:

The integrated analyses provide a solid structural and thermodynamic basis for BXD's anti-inflammatory effects in AGE. The results suggest that key BXD components can stably occupy the active sites of TNF and STAT3, potentially disrupting pathological signaling loops, which warrants future experimental exploration.

【Keywords】 Banxia Xiexin Decoction (BXD); acute gastroenteritis(AGE); network pharmacology; molecular docking; molecular dynamics simulation; MM-PBSA.

Acute gastroenteritis (AGE) is a globally prevalent gastrointestinal disorder, primarily caused by infections with bacteria, viruses, or parasites. Its typical symptoms include diarrhea, nausea, vomiting, abdominal pain, and fever. AGE can lead to severe dehydration and electrolyte imbalances, particularly in children and the elderly, making it one of the leading causes of mortality among children worldwide(1). It is estimated that approximately 3 to 5 billion cases of AGE occur globally each year, with higher incidence rates reported in low-income countries(2). Among the etiological agents, norovirus remains a predominant cause, accounting for nearly 18% of global AGE infections(3).

The pathophysiology of AGE involves complex pathological mechanisms, particularly the activation of inflammatory responses and immune pathways. During infection, pathogens stimulate major signaling cascades, including TLR4/NF-κB,

MAPK, and PI3K-Akt, leading to an excessive immune response. This response disrupts intestinal barrier function, exacerbates mucosal inflammation, and causes the overproduction of pro-inflammatory cytokines (4). Such dysregulated inflammatory signaling leads to epithelial barrier dysfunction and overproduction of pro-inflammatory cytokines, underscoring the importance of targeting intestinal mucosal inflammation pathways as a therapeutic strategy.

Current treatment options for AGE primarily rely on supportive care, including oral rehydration salts (ORS) and antibiotics. However, effective antiviral or anti-inflammatory agents remain limited. While ORS corrects dehydration, it does not inhibit pathogen replication, and inappropriate antibiotic use contributes to antimicrobial resistance. Moreover, monotherapies targeting single molecular pathways are inadequate for a multifactorial condition like AGE, where epithelial injury, immune dysregulation, and microbial imbalance coexist(5). Therefore, there is an urgent need for multi-target, multi-pathway therapeutic strategies capable of restoring intestinal homeostasis and controlling inflammation.

Banxia Xiexin Decoction (BXD) is a classical traditional Chinese medicine (TCM) prescription widely used for gastrointestinal disorders. It has demonstrated significant clinical efficacy in the treatment of gastritis, gastric ulcers, and gastrointestinal functional dysregulation. BXD is composed of seven herbs: Pinellia ternata (Banxia), Coptis chinensis (Huanglian), Scutellaria baicalensis (Huangqin), Zingiber officinale (Ganjiang), Panax ginseng (Renshen), Glycyrrhiza uralensis (Gancao), and Ziziphus jujuba (Dazao). Pharmacologically, BXD exerts multiple effects, including heat clearance, detoxification, stomach harmonization, qi regulation, and antiemetic actions(6). Recent studies indicate that BXD modulates gastrointestinal immunity, regulates the intestinal microenvironment, and enhances mucosal barrier repair, thereby alleviating AGE-related symptoms(7).

With the advancement of systems pharmacology and computational simulation, techniques such as network pharmacology, molecular docking, and molecular dynamics (MD) simulations, researchers now have new tools to investigate the multi-component and multi-target nature of TCM formulas. These methods provide system-level insights

into the interactions between complex herbal ingredients and biological networks, allowing for the prediction of potential targets and signaling pathways (8). Network pharmacology integrates information on chemical composition, target prediction, and pathway analysis, facilitating the elucidation of holistic mechanisms of TCM formulas in disease treatment(9). Molecular docking can precisely simulate the interactions between active compounds and target proteins, evaluating their binding affinity and potential bioactivity(10). Molecular dynamics simulations further enable real-time, atomistic-level analysis of drug–target complex stability and conformational dynamics (11). By applying these techniques, the mechanisms underlying BXD's therapeutic effects can be systematically explored, and its potential molecular targets and pathways in the treatment of gastroenteritis can be identified. This provides a new theoretical basis for the clinical application of BXD(12, 13).

In this study, we employed an integrated computational framework to explore the AGE-specific pharmacological mechanisms of BXD. Active compounds from BXD were screened from the TCMSP and SwissADME databases according to ADME criteria, while disease-related targets were collected from GeneCards, OMIM, CTD, and TTD. Common targets were identified and analyzed via Cytoscape-based network topology and STRING-based protein–protein interaction (PPI) analysis to determine key hub genes. GO and KEGG enrichment analyses were performed to highlight the biological processes and signaling pathways underlying BXD’s anti-inflammatory and mucosal-protective effects. The top hub targets and key compounds were subsequently validated through molecular docking and 100 ns MD simulations to evaluate complex stability. This integrative workflow (Figure 1) provides a systems-level overview of the multi-target, multi-pathway mechanisms through which BXD may exert protective effects against AGE.

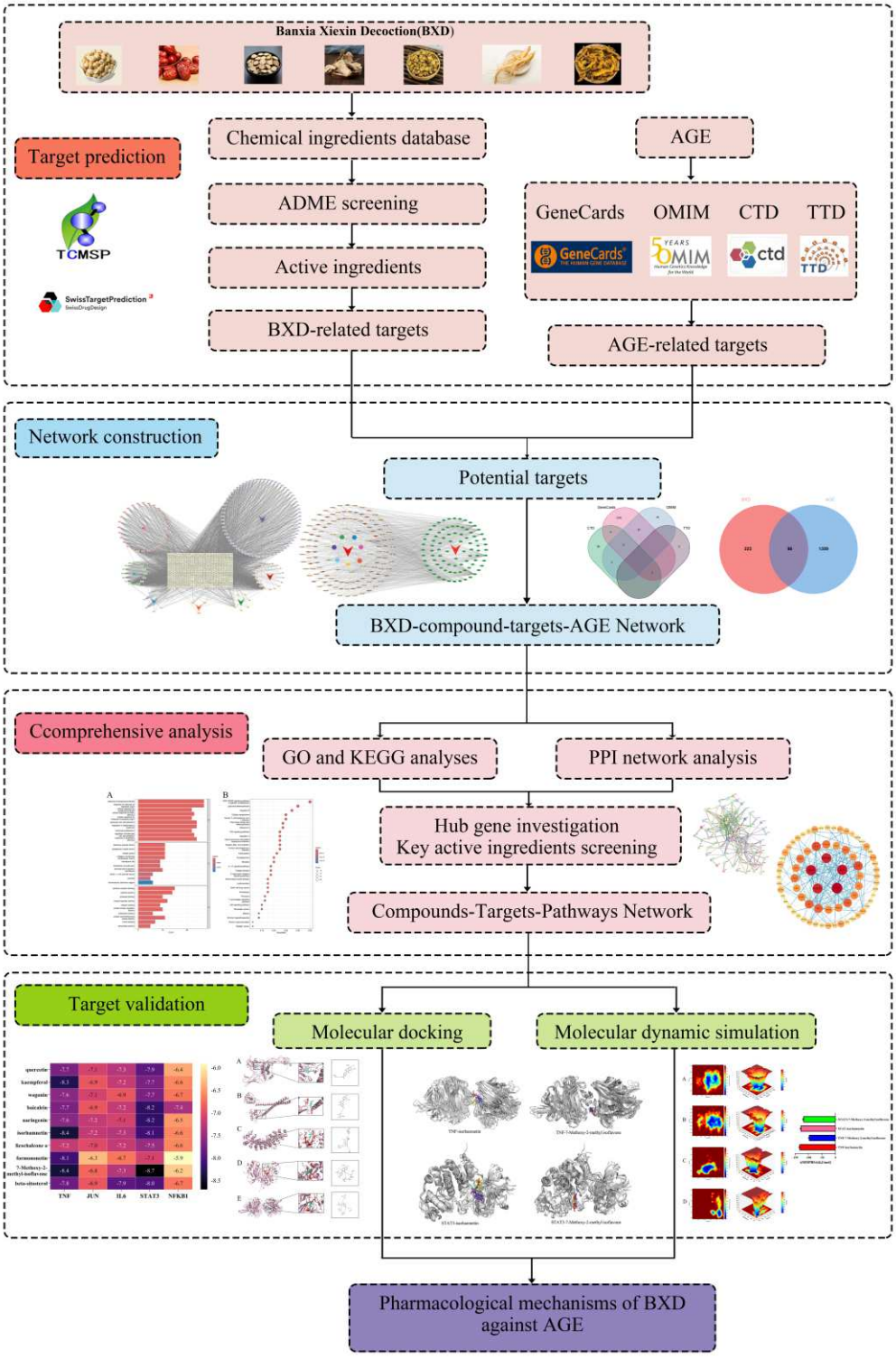


Figure 1. Research Technology Roadmap

1 Materials and Methods

1.1 Screening of Active Compounds and Potential Targets of BXD

The chemical constituents of the seven herbs in BXD—Pinellia ternata, Coptis chinensis, Scutellaria baicalensis, Zingiber officinale, Glycyrrhiza uralensis, Panax

ginseng, and Ziziphus jujuba—were collected. Based on pharmacokinetic parameters, the Traditional Chinese Medicine Systems Pharmacology Database (TCMSP, https://tcmspw.com/tcmsp.php) was used to retrieve the active components of the seven herbs. The screening criteria were set as oral bioavailability (OB) ≥ 30% and drug-likeness (DL) ≥ 0.18(14). which are widely adopted parameters in network pharmacology studies to ensure the selection of compounds with favorable ADME profiles and drug-like characteristics(9, 15). Compounds without predicted targets were excluded, yielding a final list of active ingredients.

To ensure comprehensive coverage of pharmacologically relevant constituents, compounds with experimentally reported bioactivities related to inflammation or gastrointestinal protection—yet absent from the TCMSP database—were manually supplemented through literature validation. Each manually added compound was supported by peer-reviewed evidence and is described in the Results section (Table 2), where herb source, OB/DL values (if available), and corresponding literature reference. Moreover, literature validation further confirmed that several TCMSP-screened compounds, such as isorhamnetin, acacetin, and diosmetin, have been experimentally demonstrated to exert anti-inflammatory and mucosal-protective effects in intestinal models, thereby supporting the reliability and biological relevance of our compound selection.

1.2 Prediction of Acute Gastroenteritis-Related Targets

Disease-related targets for acute gastroenteritis were identified by querying the GeneCards (https://www.genecards.org/), OMIM (https://www.omim.org/), TTD (http://db.idrblab.net/ttd/), and CTD (https://ctdbase.org/) databases using the keyword “Acute Gastroenteritis.” After removing duplicate entries, all retrieved targets were integrated to construct a comprehensive target set related to gastroenteritis.

1.3 Target Prediction and Cross-Validation

To predict the potential targets of BXD active compounds, two complementary approaches were employed. First, compound–target associations were retrieved from the TCMSP database, which integrates experimentally validated and computationally predicted targets based on pharmacophore mapping and chemical similarity models. In

parallel, additional targets were predicted using the SwissTargetPrediction platform (https://www.swisstargetprediction.ch/), which estimates target probability according to 2D and 3D structural similarity to known bioactive ligands.

To enhance reliability, only human (Homo sapiens) targets with probability scores ≥ 0.1 in SwissTargetPrediction were retained. Duplicated targets predicted by both databases were merged, while inconsistent or non-protein entries (e.g., enzyme cofactors, chemical categories) were removed. All retained targets were then standardized to official gene symbols using the UniProt database (https://www.uniprot.org/), yielding a high-confidence compound–target association dataset for subsequent network construction.

1.4 Identification of Common Targets Between BXD and Acute Gastroenteritis

The gene targets of BXD active compounds obtained from Section 1.1 and the disease-related targets associated with acute gastroenteritis retrieved in Section 1.2 were uploaded to the jvenn online platform (https://jvenn.toulouse.inrae.fr/) to generate a Venn diagram. The intersecting were identified as potential therapeutic targets representing the molecular basis of BXD's activity against AGE.

1.5 Construction of the Protein–Protein Interaction (PPI) Network and Identification of Hub Targets

The overlapping targets were imported into the STRING database (https://string-db.org/) with the species parameter set to Homo sapiens and the confidence score threshold set to >0.9. Disconnected nodes were hidden to generate a reliable protein–protein interaction (PPI) network. The resulting network data were exported in tab-separated values (TSV) format and imported into Cytoscape 3.10.3 for visualization and further analysis.

To explore the network structure in depth, key topological parameters including degree centrality (DC), closeness centrality (CC), and betweenness centrality (BC) were calculated. By applying appropriate threshold values, hub targets with significant centrality were identified, ensuring that the selected targets were of high importance within the network. The CytoHubba plugin of Cytoscape was then used to visually present the complex interactions among these core genes.

1.6 Gene Ontology (GO) and Kyoto Encyclopedia of Genes and Genomes (KEGG)

Enrichment Analysis

To further elucidate the biological functions of the identified hub targets, we conducted functional enrichment analysis using the DAVID database. The species was set to Homo sapiens, and both Gene Ontology (GO) and Kyoto Encyclopedia of Genes and Genomes (KEGG) data associated with the targets were retrieved.

To ensure the statistical significance of the enrichment results, thresholds were set at p-value < 0.05 and false discovery rate (FDR) < 0.05 (16). Based on these criteria, the top 10 enriched GO terms were extracted, covering the three major categories: Biological Process (BP), Molecular Function (MF), and Cellular Component (CC). A circle plot was generated using the ggplot2 package in R to visualize the degree of enrichment and significance of each GO term.

Similarly, the top 10 significantly enriched KEGG pathways were identified and visualized using a bubble plot, which presented the significance level, number of involved genes, and enrichment score of each pathway. These analyses provided insights into the roles of the core targets in biological processes and their involvement in key signaling pathways.

1.7 Construction of the Compound–Target–Pathway Network

Based on the results of active ingredient screening and KEGG enrichment analysis, a compound–target–pathway network for BXD was constructed using Cytoscape. The network was built by integrating the relationships between active compounds and intersecting targets, and further incorporating significantly enriched KEGG pathways. This multi-dimensional regulatory network highlights the interactions among key components, core targets, and critical signaling pathways, thereby providing a systematic overview of the potential mechanisms of BXD in the treatment of acute gastroenteritis.

1.8 Molecular Docking

The molecular structures of the top ten active compounds were retrieved from the PubChem database (https://pubchem.ncbi.nlm.nih.gov/) and downloaded in SDF format. To ensure structural accuracy, each ligand was subjected to minimization using Chem3D, optimizing molecular conformation and reducing internal strain before

docking. The minimized structures were then converted into MOL2 format for subsequent analysis.

Three-dimensional crystal structures of the top five target proteins were obtained from the RCSB PDB database (https://www.rcsb.org/). Selecting high-resolution entries that contained bound ligands for accurate active-site definition. All protein structures were preprocessed using PyMOL 3.1.1, included removal of water molecules, addition of hydrogen atoms, and correction of missing residues or atoms. The GetBox plugin was employed to define the docking coordinates based on the position of the co-crystallized ligand, and the native ligands were subsequently removed to prepare the receptors.

Molecular docking was performed using AutoDock Vina (version 1.2.3), which employs a hybrid scoring function combining empirical free-energy terms and gradient-based local optimization. Default exhaustiveness parameters were used unless otherwise stated. Binding affinity (kcal/mol) was calculated for each docking pose, and the most stable conformation with the lowest binding energy was selected for further visualization and analysis. To evaluate docking reliability, redocking validation was conducted by re-docking the original co-crystallized ligands into their respective receptor binding sites using the same grid box parameters. The RMSD between the redocked and crystallographic poses was computed automatically by Vina. The best docking mode showed an RMSD of 0.000 Å, indicating perfect pose reproduction. According to established criteria, an RMSD $\leq$ 2.0 Å confirms docking precision and methodological reliability(17).

Finally, docking results were visualized using PyMOL and Discovery Studio Visualizer, highlighting hydrogen bonds, hydrophobic contacts, and electrostatic interactions within the active sites. These results provide theoretical support for understanding the molecular mechanisms by which Banxia Xiexin Decoction may exert therapeutic effects in the treatment of acute gastroenteritis.

1.9 Molecular Dynamics Simulation

To further validate the stability and binding dynamics of the protein–ligand complexes obtained from molecular docking, MD simulations were performed using

GROMACS 2024.2. As a key tool in structural bioinformatics, MD simulations can reveal the physical behavior of molecular systems at near-atomic resolution under defined conditions, playing a critical role in elucidating drug–target interaction mechanisms. The resulting data offer multidimensional insights, including complex stability, conformational changes, energy variations, and key interaction residues, thereby providing quantitative support for pharmacodynamic studies (18).

In this study, the amber99sb-ildn.ff force field was employed to generate topology parameters for the protein, owing to its robust performance in handling flexible protein conformations. For the ligands, GAFF2 (General AMBER Force Field 2) parameters were generated using the sobtop toolkit (v1.0). Partial atomic charges were assigned using the AM1-BCC semi-empirical method, ensuring a balance between accuracy and computational efficiency. Parameter validation included topology consistency checks and atom-type mapping verification to ensure correct ligand–protein integration prior to simulation.

Each complex was solvated in a dodecahedral periodic box with at least 1.0 nm distance from the solute to the box edge, using the SPC/E water model. Counterions were added to neutralize the system, ensuring charge balance and physical realism (19). Energy minimization was performed via the steepest descent algorithm until the maximum force converged below 1000 kJ/mol/nm. Subsequently, NVT (constant volume and temperature) and NPT (constant pressure and temperature) equilibrations were performed for 100 ps each, stabilizing the systems at 310 K and 1 bar. Temperature coupling was achieved using the V-rescale thermostat (τT = 0.1 ps), and pressure coupling employed the Parrinello–Rahman barostat (τP = 2.0 ps) with a compressibility of 4.5×10^{-5} bar^{-1}. Positional restraints were gradually released during equilibration.

Production MD simulations were run for 100 ns with a 2 fs time step. Long-range electrostatic were computed with the Particle Mesh Ewald (PME) method, while van der Waals forces were treated using a force-switch cutoff of 1.0 nm, ensuring accurate treatment of electrostatic shielding and non-bonded interactions (20). The LINCS algorithm was applied to constrain hydrogen bonds, improving computational efficiency and system stability. Trajectory data, including energy, coordinates, and logs,

were saved every 50,000 steps for subsequent analysis.

The dynamic stability of the complexes was assessed using root-mean-square deviation (RMSD), root-mean-square fluctuation (RMSF), radius of gyration (Rg), solvent-accessible surface area (SASA), and hydrogen bond occupancy, which are standard descriptors of conformational stability and binding robustness (21, 22). structures were extracted at representative time points (0, 25, 50, 75, and 100 ns) to examine the evolution of ligand binding modes and conformational adaptation.

To further evaluate the binding behavior, binding free energies were calculated using the MM-PBSA approach implemented in the g_mmpbsa package. The last 10 ns (90–100 ns) of each trajectory were analyzed, extracting one frame every 100 ps (totaling 100 frames), and the average binding free energy was reported as mean ± standard deviation to ensure energetic convergence. This analysis provided thermodynamic validation of the docking and MD results, ensuring consistency across computational methods (23, 24).

2.Result

2.1 Active Compounds and Potential Targets of BXD

A total of 144 active compounds in BXD were obtained after database screening and removal of duplicates, among which 12 compounds were shared by multiple herbs, indicating potential synergistic pharmacological effects. In total, 308 potential targets were identified. Detailed information on the active compounds and its corresponding targets from the seven herb is provided in Table 1.

To ensure the pharmacological relevance of the screened compounds, literature validation was performed for representative flavonoids and alkaloids retrieved from TCMSP. Several key compounds, including isorhamnetin, acacetin, and diosmetin, have been experimentally reported to exhibit anti-inflammatory and mucosal-protective activities in gastrointestinal models, supporting the reliability and biological plausibility of our compound selection (Table 2).

The herb–compound–target interaction network was constructed and visualized in Figure 2. In this network, A1–A12 represent the 12 common active compounds, while the capital letters denote the initials of each herb in BXD. The active compounds specific to individual herbs are labeled by combining the herb's initial with a unique

number (e.g., BX1, HQ1), facilitating intuitive tracking of compound origin and target relationships.

Table 1. Number of Active Compounds and Potential Targets in Each Herb of BXD

Herb	No. of Active Compounds	No. of Potential Targets
Pinellia ternata	10	95
Coptis chinensis	11	180
Scutellaria baicalensis	32	105
Zingiber officinale	5	45
Glycyrrhiza uralensis	69	249
Jujube	19	208
Panax ginseng	17	120

Table 2. Literature-based validation

Compound Name	Herb	OB (%)	DL	Pharmacological Relevance	Reference
Isorhamnetin	Glycyrrhiza uralensis	49.7	0.31	Attenuates chemically induced colitis via pregnane X receptor–mediated suppression of TNF-α and NF-κB signaling.	(25)
Acacetin	Scutellaria baicalensis	37.8	0.24	Inhibits NF-κB and Akt activation, thereby reducing cytokine release and protecting epithelial tissues from inflammation.	(26)
Diosmetin	Coptis chinensis	41.4	0.26	Suppresses LPS-induced IL-6, TNF-α, and COX-2 expression, exerting anti-colitic and mucosal-protective effects.	(27)
Genkwanin	Scutellaria baicalensis	38.6	0.21	Reduces pro-inflammatory cytokine production and oxidative stress while enhancing intestinal barrier integrity via Nrf2/HO-1 signaling.	(28)
5-Demethylnobiletin	Zingiber officinale	46.2	0.28	Reduces pro-inflammatory cytokine production and oxidative stress while enhancing intestinal barrier integrity via Nrf2/HO-1 signaling.	(29)

Note: Some compounds, such as diosmetin and 5-demethylnobiletin, are included as literature-validated flavonoids with strong anti-inflammatory relevance, although they may not represent the major constituents of the corresponding herbs in Banxia Xiexin Decoction.

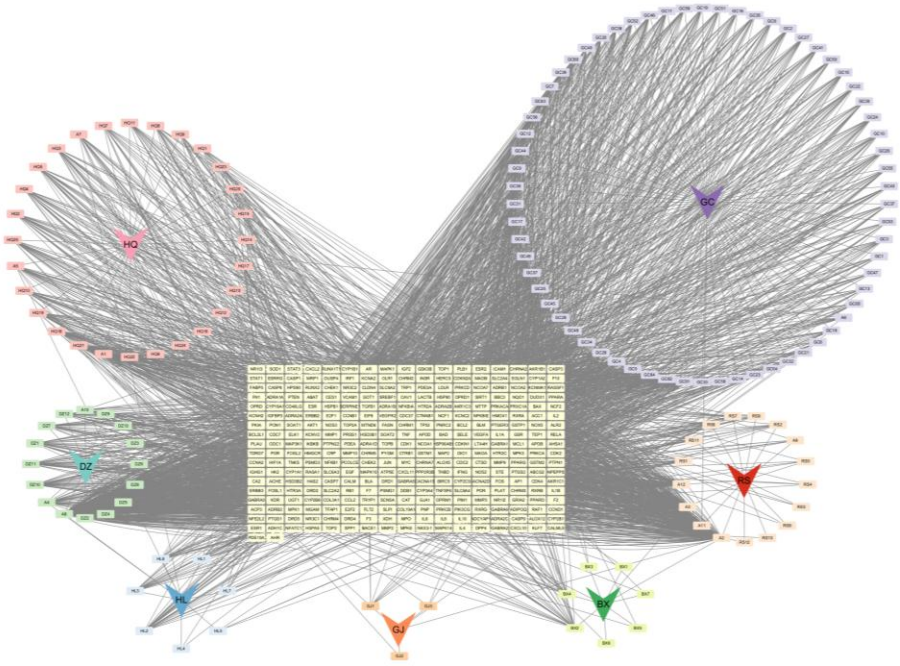


Figure 2. Network of BXD herbs, active components, and potential targets

2.2 Collection of Disease-Related Targets and Identification of Intersection Targets

A comprehensive search was conducted across multiple databases, yielding 1,303 disease-associated targets from GeneCards, 177 from the Comparative Toxicogenomics Database (CTD), 62 from the Online Mendelian Inheritance in Man (OMIM), and 9 from the Therapeutic Target Database (TTD). After integrating and deduplicating these datasets, a total of 1,445 unique acute gastroenteritis-related targets were identified. The distribution of these targets is presented in the disease-target Venn diagram (Figure 3). Subsequently, an intersection analysis was performed between the predicted targets of BXD and the disease-associated targets, resulting in 86 overlapping targets. These shared targets likely represent the critical nodes through which BXD exerts its therapeutic effects. The overlap between drug and disease targets is illustrated in the drug-disease Venn diagram (Figure 4).

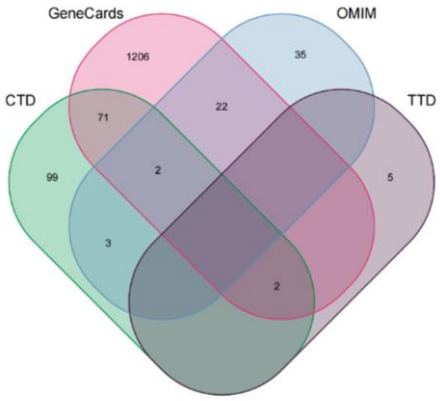


Figure 3. Venn diagram of AGE

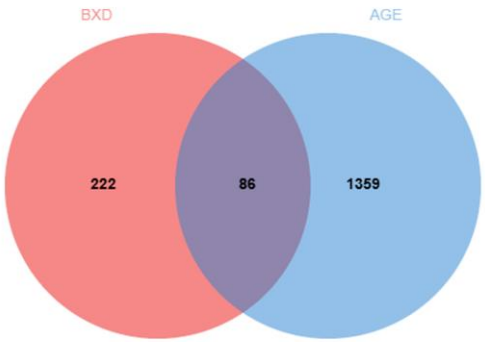


Figure 4. Venn diagram of drug-disease targets

2.3 Protein-Protein Interaction (PPI) Network Construction and Core Target Screening

To elucidate the potential mechanisms by which BXD exerts therapeutic effects on AGE, 86 intersecting targets were imported into the STRING database (https://string-db.org) with the organism set to Homo sapiens. A protein-protein interaction (PPI) network was generated using a high confidence score threshold (>0.9). The resulting network contained 73 nodes and 248 edges, with an average node degree of 5.3, indicating strong interconnectivity among the candidate targets (Figure 5).

The PPI network data were subsequently exported in TSV format and visualized in Cytoscape 3.10.1. Topological analysis was performed with the CytoNCA plugin based on betweenness centrality (BC), closeness centrality (CC), and degree centrality (DC). By applying a three-step screening strategy—retaining nodes above the median values of all three parameters at each iteration—five core regulatory targets were identified: tumor necrosis factor (TNF), transcription factor AP-1 component (JUN), interleukin-6 (IL6), signal transducer and activator of transcription 3 (STAT3), and nuclear factor κB subunit 1 (NFKB1) (Figure 6, Table 3).

These hub targets are closely associated with inflammatory signaling, immune regulation, and cellular stress responses, all of which play central roles in the pathogenesis of AGE. Collectively, these findings suggest that BXD may exert its therapeutic effects through multi-target synergistic modulation of these inflammation-related signaling pathways.

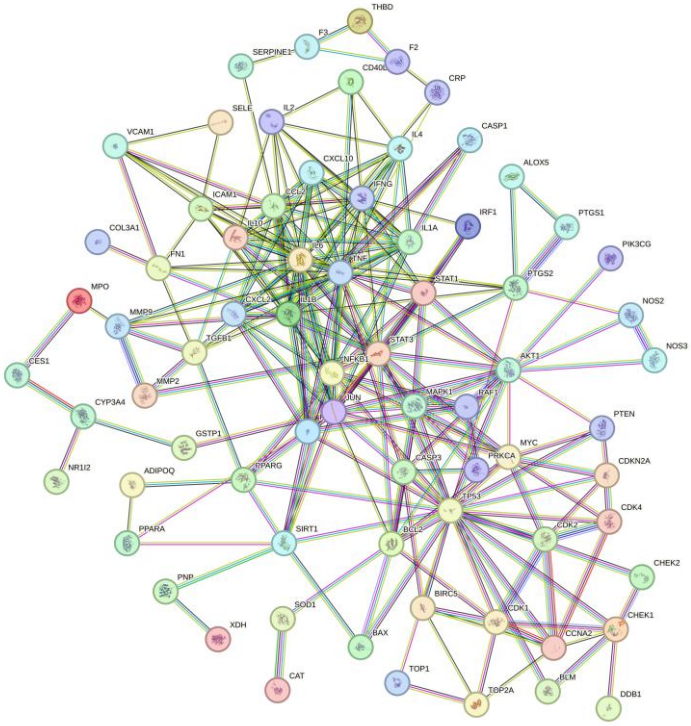


Figure 5. PPI network diagram.

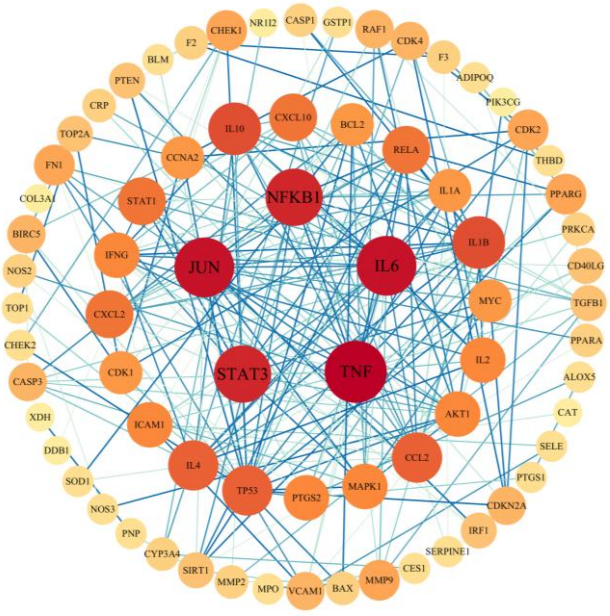


Figure 6. Core targets of BXD in the treatment of AGE.

Table 3 Topological Parameters of Core Targets

Target Name	DC	CC	**BC**
TNF	25	0.8000	55.81
JUN	14	0.7692	36.67
IL6	14	0.7692	35.11
STAT3	13	0.7407	33.10
NFKB1	13	0.7407	29.67

2.4 Gene Ontology (GO) and Kyoto Encyclopedia of Genes and Genomes (KEGG) Enrichment Analysis

Candidate targets identified were imported into the DAVID database for GO functional enrichment analysis. A total of 312 Biological Process (BP) terms, 62 Cellular Component (CC) terms, and 97 Molecular Function (MF) terms related to BXD treatment of AGE were significantly enriched. For improved visualization, the top 10 enriched terms from each category were selected for further analysis and presented as bar plots (Figure 7).

In the MF category, significantly enriched functions included peroxidase activity (GO:0004601), protein kinase regulator activity (GO:0019887), heme binding (GO:0020037), and cytokine receptor binding (GO:0005126), indicating that the candidate targets are involved in redox regulation, cytokine binding, and signal transduction. Additionally, enrichment in integrin binding and immune receptor binding suggests that these targets may regulate cell adhesion and immune cell activation, processes closely linked to intestinal epithelial repair and mucosal immunity.

Within BP, the most enriched terms were response to bacterial molecular patterns such as lipopolysaccharide (GO:0071222), response to inflammatory stimulus (GO:0006954), leukocyte proliferation (GO:0070661), and immune system regulation (GO:0002682). These processes are directly associated with innate immune activation and inflammatory signaling in the intestinal mucosa, implying that BXD may alleviate AGE symptoms by modulating epithelial immune responses and suppressing pro-inflammatory mediators.

In the CC category, candidate targets were mainly enriched in cytosol (GO:0005829), plasma membrane external side (GO:0009897), cytoplasmic vesicle

lumen (GO:0060205), secretory granule lumen, and membrane microdomains. This distribution suggests that these targets are predominantly localized in sites of cytokine secretion and membrane signaling, supporting their involvement in intercellular communication and mucosal defense.

KEGG pathway enrichment analysis revealed that candidate targets were predominantly involved in multiple inflammation-, immunity-, and infection-related pathways. Notably enriched pathways included the TNF signaling pathway (hsa04668), IL-17 signaling pathway (hsa04657), T cell receptor signaling pathway (hsa04660), Th17 cell differentiation (hsa04659), and Inflammatory Bowel Disease (IBD) pathway (hsa05321). These pathways play essential roles in intestinal mucosal immune regulation, epithelial barrier maintenance, and chronic inflammation, indicating that BXD may exert protective effects through coordinated regulation of cytokine networks and epithelial immune balance. Importantly, the enrichment of mucosa-associated pathways such as the “intestinal immune network for IgA production” and “tight junction regulation” (detected in subsequent analysis) further supports the hypothesis that BXD promotes gut barrier homeostasis in AGE..

Additionally, enrichment was observed in the AGE-RAGE signaling pathway (hsa04933), p53 signaling pathway (hsa04115), and HIF-1 signaling pathway (hsa04066), which are closely associated with oxidative stress responses, epithelial damage repair, and inflammatory mediator expression .

In summary, GO and KEGG enrichment analyses collectively suggest that BXD exerts its therapeutic effects in AGE through multi-target modulation of intestinal immune and inflammatory pathways, enhancement of mucosal barrier integrity, and attenuation of oxidative stress–induced epithelial injury.

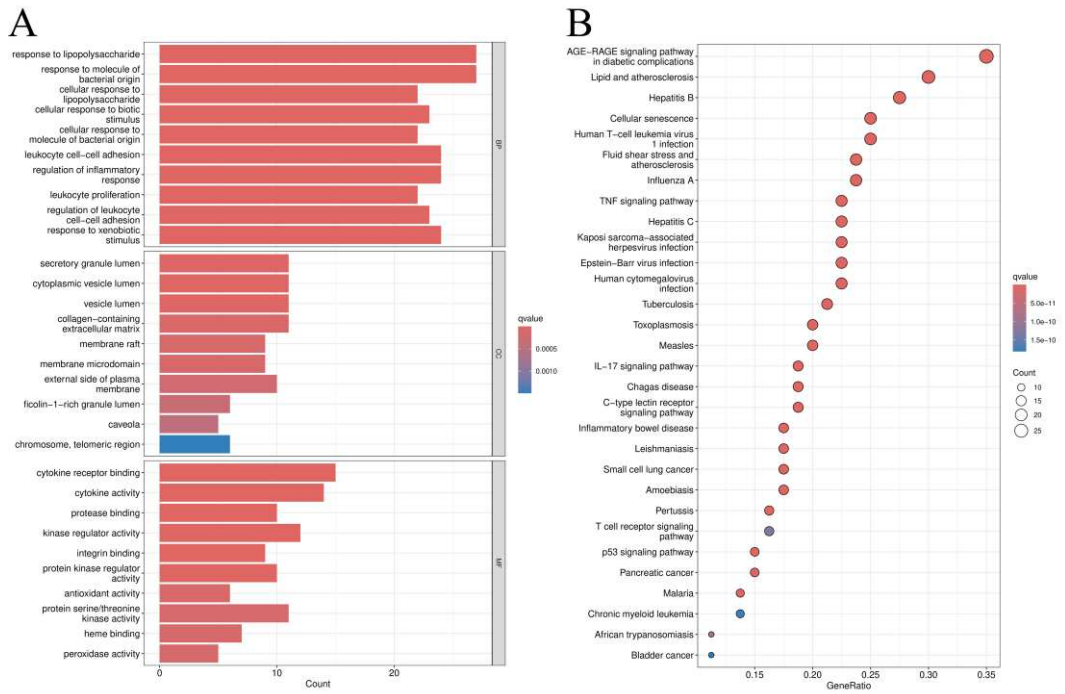


Figure 7. GO and KEGG enrichment analysis of core targets. A: Bar chart of GO functional enrichment analysis; B: Bubble chart of KEGG pathway enrichment analysis.

2.5 Topological Network Analysis of Drug–Component–Target–Pathway–Disease

Network topology analysis was performed using the Network Analyzer plugin in Cytoscape to quantitatively evaluate the centrality and connectivity of nodes within the integrated pharmacological network. The resulting visualization is presented in Figure 8.

In the constructed topological map, the left section depicts the drug BXD in red, while the seven constituent herbs of the formula are represented by green, dark blue, pink, orange, yellow, light blue, and purple, respectively. Active components are labeled with their MOL IDs and colored according to their corresponding herbs. Core active components are highlighted in green, target proteins involved in pharmacological effects are shown in blue, signaling pathways are indicated in orange, and the disease gene (AGE) is marked in green.

Topological parameter evaluation revealed that a subset of compounds exhibited strong interconnectivity with multiple targets and pathways, indicating potential multi-target regulatory capacity and system-level relevance. The top ten ranked core active components were selected for subsequent molecular docking analysis. Details of these

components are listed in Table 4.

Table 4. Information of the top ten core active compounds

MOL ID	Name	Degree
MOL000098	quercetin	70
MOL000422	kaempferol	24
MOL000173	wogonin	23
MOL002714	baicalein	18
MOL004328	naringenin	15
MOL000354	isorhamnetin	14
MOL000497	licochalcone a	14
MOL000392	formononetin	14
MOL003896	7-Methoxy-2-methyl isoflavone	13
MOL000358	beta-sitosterol	11

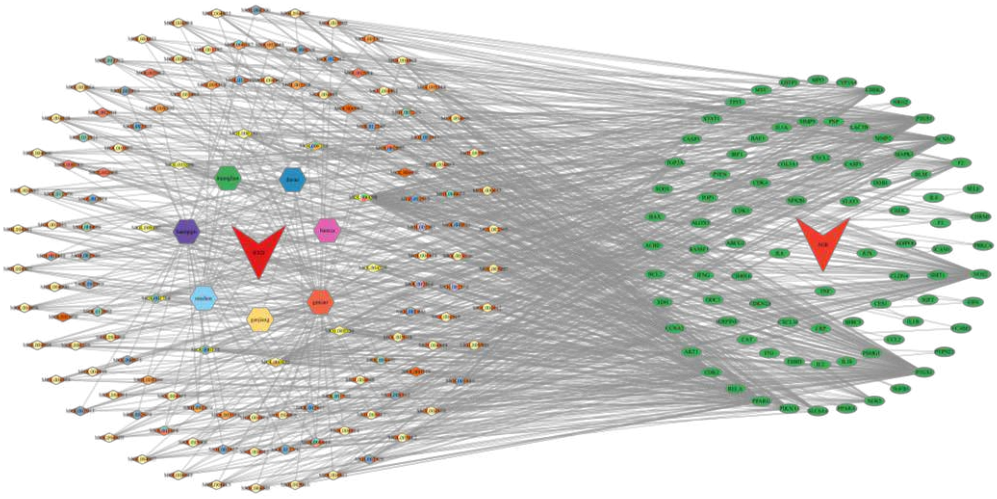


Figure 8. Topological network of drug–component–target–pathway–disease.

2.6 Molecular Docking Results

To validate the binding affinities between the screened active compounds and the key protein targets associated with AGE, molecular docking was conducted to systematically evaluate the interactions of ten major active compounds (e.g., quercetin, kaempferol, wogonin, etc.) with five core targets—TNF, JUN, IL6, STAT3, NFKB1. Lower docking scores (more negative binding energies) indicate stronger ligand-receptor binding and more stable complexes (30). According to the literature(31),

binding affinities below −4.25 kcal/mol suggest potential ligand-target interactions; below −5.0 kcal/mol indicate good binding activity; and below −7.0 kcal/mol represent strong docking affinity.

For each ligand-target pair, twenty binding poses were generated during molecular docking to comprehensively evaluate alternative binding modes. Among these, the pose with the lowest binding energy and most favorable interaction conformation was selected for visualization and further analysis. This approach ensures that the displayed results represent the most stable and biologically relevant binding modes under the docking protocol.

As summarized in Figure 9, most active compounds displayed favorable binding affinities across all five targets, ranging from −5.9 to −8.7 kcal/mol. Among them, isorhamnetin showed the strongest binding affinity to multiple targets, particularly TNF (−8.4 kcal/mol) and STAT3 (−8.1 kcal/mol), implying a potential key role in anti-inflammatory signaling regulation (32). Additionally, 7-Methoxy-2-methyl-isoflavone exhibited the lowest binding energy (−8.7 kcal/mol) with STAT3, suggesting its involvement in modulating this signaling axis for anti-inflammatory immune regulation. Quercetin and kaempferol showed robust binding with all targets, especially with inflammatory mediators such as TNF, IL6, and STAT3, consistent with previous reports of their regulation of cellular inflammatory responses via MAPK and NF-κB pathways (33).Wogonin and baicalein also displayed strong affinities with STAT3 and NFKB1, indicating potential synergistic regulation of Th17, NF-κB, and other inflammation-related pathways in the gastrointestinal tract (34). β-Sitosterol demonstrated a notable binding affinity to IL6 (−7.9 kcal/mol), suggesting its possible involvement in mucosal protection via the downregulation of pro-inflammatory cytokines (35).

Figure 10 illustrates the three-dimensional structural visualization of the optimal ligand–protein complexes for five target proteins, performed using PyMOL. The figure clearly illustrates the key intermolecular interactions between the ligands (green) and their corresponding protein receptors (pink), including hydrogen bonding, hydrophobic interactions, and electrostatic forces. Each complex is magnified to highlight the binding conformation of the ligand within the active site of the receptor, as well as the

specific interactions with surrounding amino acid residues (red). The number and positions of hydrogen bonds (yellow dashed lines) formed between ligands and receptors are explicitly marked, and Each binding pocket is shown with a close-up view, and the corresponding 2D interaction diagrams clearly label hydrogen bonds (yellow dashed lines), hydrophobic contacts, and π-stacking interactions, thus facilitating interpretation of the binding mode.

Detailed analysis revealed that IL6–7-Methoxy-2-methyl-isoflavone forms hydrogen bonds with SER229; JUN–naringenin interacts with ASP99 (hydrogen bond) and ARG345 (π-stacking); baicalein–NFKB1 forms hydrogen bonds with ASN235 and SER234 and π–π stacking with TRP273; STAT3–7-Methoxy-2-methyl-isoflavone is stabilized by hydrogen bonding with SER234 and electrostatic contacts with ARG182 and ARG185; and isorhamnetin–TNF involves hydrogen bonds with ASN275, SER179, and THR165, potentially interfering with receptor activation.

Collectively, these findings demonstrate that multiple active components in BXD can form stable and energetically favorable complexes with key inflammatory targets, supporting a multi-target synergistic mechanism underlying its anti-inflammatory effects. This molecular evidence provides a structural foundation for subsequent molecular dynamics simulations and mechanistic validation.

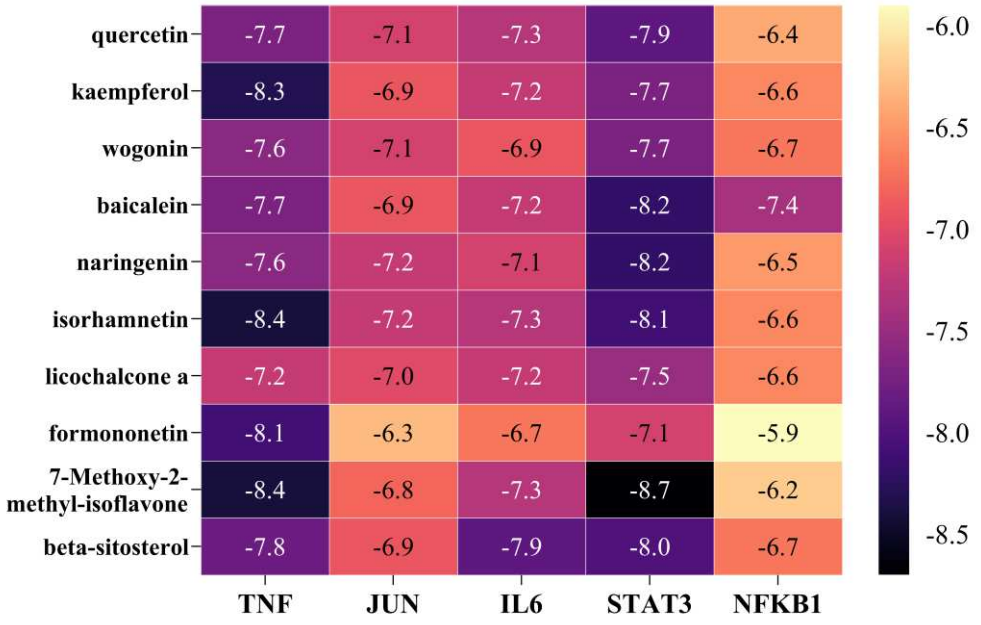


Figure 9. Binding energy scores (kcal/mol) of molecular docking between core active compounds

and key target proteins.

Abbreviations: TNF, tumor necrosis factor; JUN, transcription factor AP-1; IL6, interleukin-6; STAT3, signal transducer and activator of transcription 3; NFKB1, nuclear factor kappa-B subunit 1

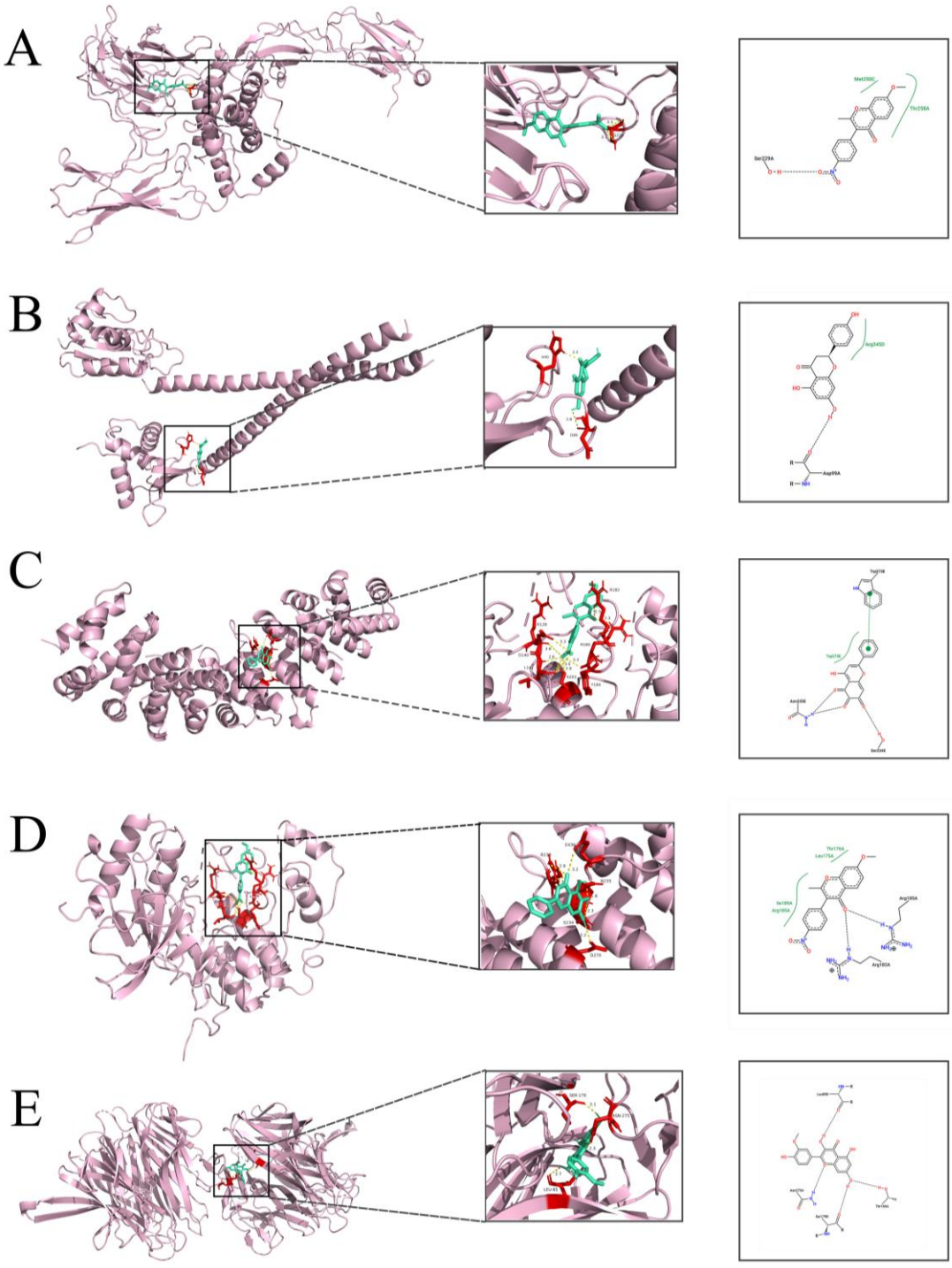


Figure 10. Visualization of molecular docking between major core compounds and key target proteins. A：IL6-(7-Methoxy-2-methyl isoflavone)；B：JUN-naringenin；C：NFKB1-baicalein；D：STAT3-(7-Methoxy-2-methyl isoflavone)；E：TNF-isorhamnetin

2.7 Molecular Dynamics Simulation Results

To overcome the limitations of rigid protein assumptions in molecular docking and further validate the binding stability between core active compounds and key targets, this study selected two key compounds with low binding energies—7-Methoxy-2-methyl-isoflavone and isorhamnetin—were subjected to100 ns MD simulations with their respective core targets, STAT3 and TNF, resulting in four complex systems in total.

Figure 11 presents key dynamic parameters including RMSD, RMSF, Rg, SASA, and hydrogen bond occupancy, which were used to evaluate the stability and compactness of the complexes. As shown in Figure 11, RMSD curves of all four complexes stabilized within the first 20 ns, with the STAT3–7-Methoxy-2-methyl-isoflavone complex exhibiting the smallest fluctuation range (approximately 0.5–1.0 nm), indicating strong preference conformational stability. RMSF analysis revealed generally low fluctuations (<1.5 nm) except for a few flexible loop residues, suggesting ligand binding did not significantly perturb the protein backbone. Both Rg and SASA profiles showed minimal variation, reflecting stable and compact protein folding throughout the simulation. Hydrogen bond analysis indicated the presence of multiple stable hydrogen bonds in all systems, with the STAT3–7-Methoxy-2-methyl-isoflavone complex maintaining the highest hydrogen bond count, implying stronger ligand-target interactions.

Figure 12 and Table 4 summarize the MM-PBSA binding free energy decomposition results for the four complexes. Electrostatic and van der Waals interactions were the dominant driving forces for ligand binding, with the TNF–isorhamnetin complex showing the most favorable binding free energy at (-133.97±12.83 kJ/mol), in good agreement with its stable hydrogen bond network. The calculated mean binding free energies (mean ± SD) were consistent with the energetic trends observed in docking, confirming methodological consistency and reliability between docking and MD simulations.

Furthermore, per-residue energy decomposition was performed to identify the key amino acid residues responsible for ligand binding (Figure 13). Both STAT3 and TNF complexes were stabilized by a combination of hydrophobic and polar interactions, with multiple residues contributing significantly to the total binding energy. In the STAT3–7-Methoxy-2-methyl-isoflavone complex, LEU189 (–11.42 kJ/mol), ILE184,

and ARG179 were the dominant contributors, forming a stable hydrophobic pocket and hydrogen bond network with the ligand. Similarly, in the TNF–isorhamnetin complex, residues such as PHE109 (–11.81 kJ/mol), ILE158, and SER179 formed extensive van der Waals and electrostatic interactions. Notably, in all four complexes, the ligand molecule itself (MOL) showed a substantial binding energy contribution due to its favorable shape complementarity and charge distribution, further confirming the results from MM-PBSA total energy analysis. These findings highlight the importance of specific binding site residues in mediating ligand stabilization and suggest potential mutational hotspots or pharmacophore targets for future optimization.

To further explore the conformational energy landscape during dynamics, free energy landscapes were constructed based on RMSD and Rg metrics (Figure 14). All four complexes exhibited distinct low-energy basins, particularly the STAT3–7-Methoxy-2-methyl-isoflavone system, which showed a single, well-defined energy minimum in the 2D landscape (marked in the figure), indicating a propensity to adopt stable conformations during simulation. The 3D free energy landscape also depicted clear energy wells, further confirming thermodynamic stability.

Additionally, Figure 15 presents the superimposed structures of each complex at 0, 25, 50, 75, and 100 ns time points. The ligand molecules remained tightly bound within their initial binding pockets without significant drift or dissociation over the simulation duration, validating the stability and reliability of their binding modes.

In summary, the molecular dynamics simulation results corroborate the docking data, confirming TNF and STAT3 as crucial targets mediating the pharmacological effects of BXD. Among these, the TNF–isorhamnetin complex demonstrated the highest stability and strongest binding affinity, warranting further investigation through experimental validation.

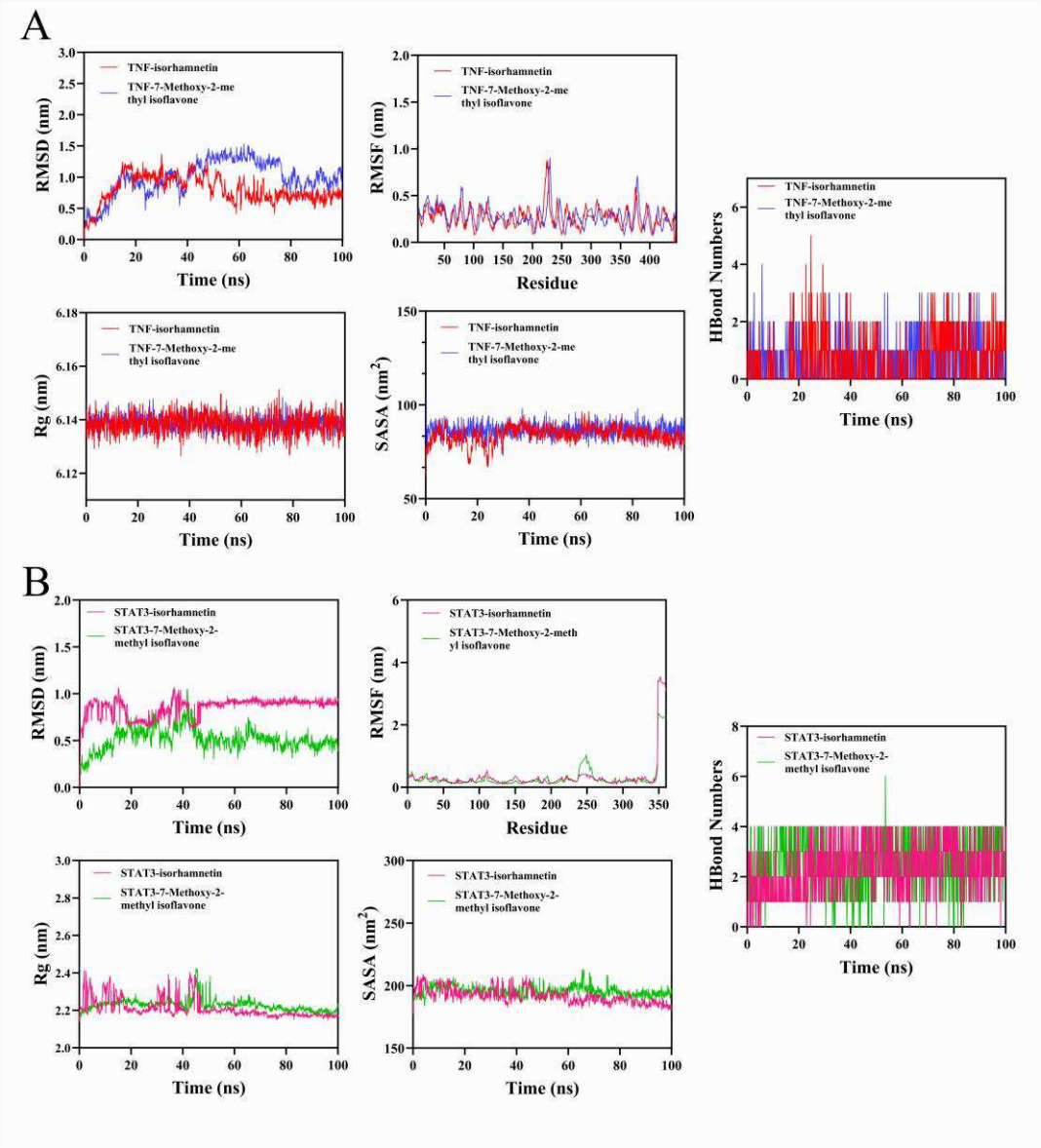


Figure 11. RMSD, RMSF, Rg, SASA, and hydrogen bond number variation curves. A: MD simulations of TNF protein with respective ligands ;B: MD simulations of STAT3 protein with respective ligands.

Table 4. Binding free energies (ΔG, mean ± SD; kJ/mol) from MM-PBSA analysis of the four protein–ligand complexes.

Complex	Δ_{GGAS}	Δ_{GSOLV}	Δ_{TOTAL}
STAT3–7-Methoxy-2-methyl-isoflavone	-217.82±17.83	98.05±7.54	-119.77±9.73
STAT3–isorhamnetin	-198.48±14.42	69.10±6.28	-129.39±11.48
TNF–7-Methoxy-2-methyl-isoflavone	-185.14±19.36	66.83±6.67	-98.31±8.79
TNF–isorhamnetin	-194.99±17.51	61.03±5.23	-133.97±12.83

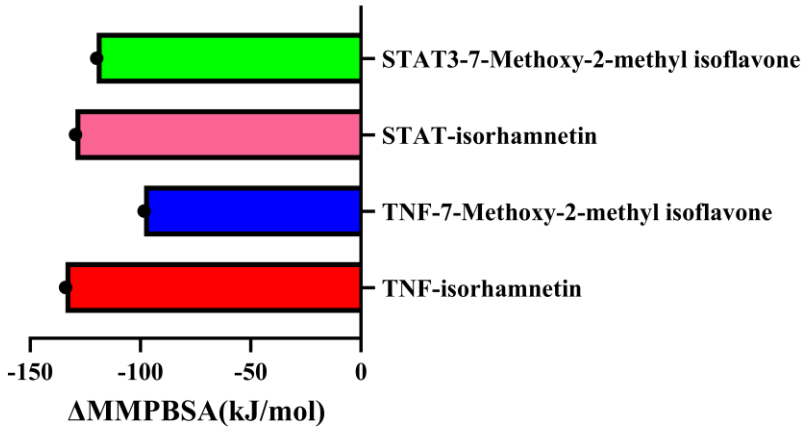


Figure 12. MM-PBSA binding free energy decomposition analysis of the four core compound–target complexes.

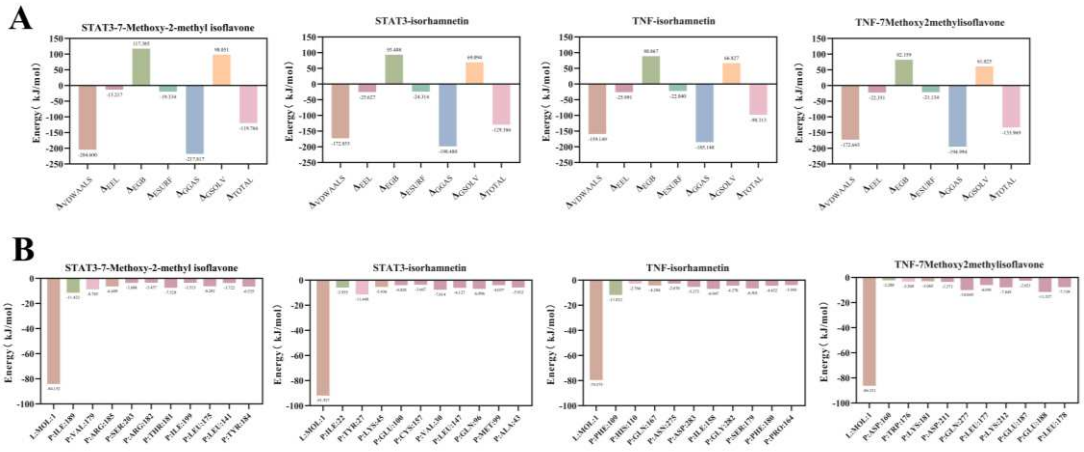


Figure 13. A: MM-PBSA energy decomposition profiles for the four protein–ligand complexes: STAT3–7-Methoxy-2-methyl-isoflavone, STAT3–isorhamnetin, TNF–7-Methoxy-2-methyl-isoflavone, and TNF–isorhamnetin. Individual energy terms include van der Waals energy (ΔVDWAALS), electrostatic energy (ΔEEL), polar solvation energy (ΔGGB), non-polar solvation energy (ΔGSURF), and total binding free energy (ΔTOTAL).
B: Per-residue free energy decomposition results. Each bar represents the contribution of the ligand (MOL) and the top 10 interacting protein residues (in kJ/mol). Negative values indicate stabilizing interactions. All four complexes showed key residues that significantly contribute to binding.

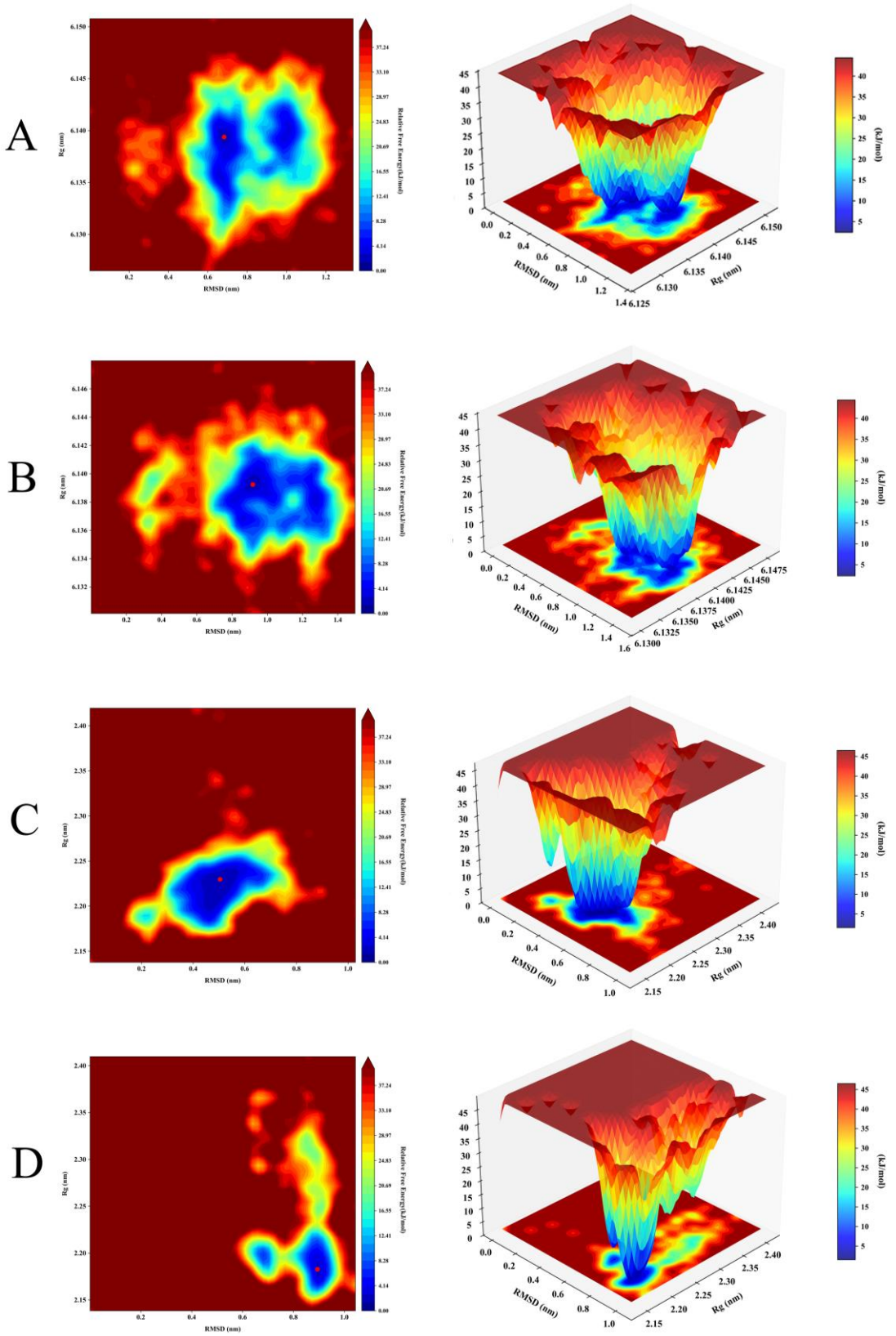


Figure 14. Free Energy Landscape (FEL) Maps. A：TNF-isorhamnetin; B：TNF-7-Methoxy-2-methyl isoflavone; C：STAT3-isorhamnetin; D：STAT3-7-Methoxy-2-methyl isoflavone
The darker (blue) regions represent lower free-energy basins, indicating energetically favorable conformations.

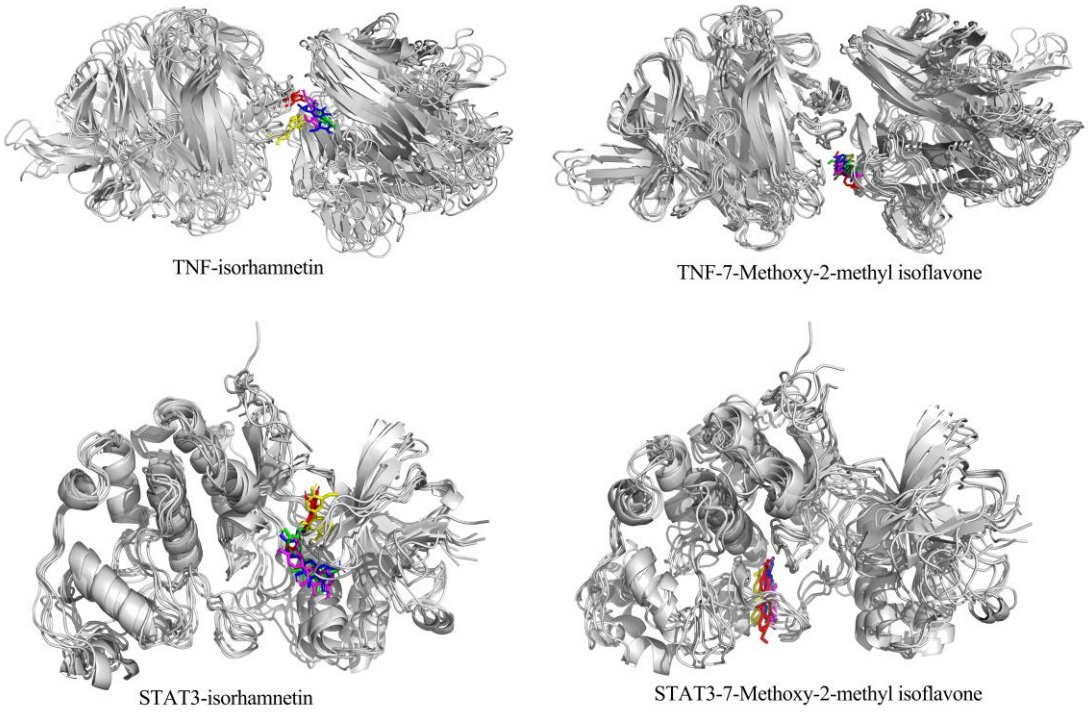


Figure 15. Binding Conformation Comparison at 0, 25, 50, 75, and 100 ns During Molecular Dynamics Simulation. Gray regions represent the TNF and STAT3 proteins. The small molecules shown in red, yellow, blue, green, and purple correspond to the ligand conformations at 0, 25, 50, 75, and 100 ns, respectively. The consistent ligand positioning across time points reflects stable binding and minimal conformational drift throughout the simulation.

3. Discussion

In this study, based on integrated target prediction and network pharmacology analyses combined with protein–ligand network topology exploration, STAT3 and TNF were identified as central targets regulating key inflammatory pathways involved in AGE, demonstrating both high topological importance and biological relevance. KEGG enrichment analysis also suggested that these two targets are involved in multiple AGE-related signaling pathways, including the “IL-6–JAK–STAT3 signaling pathway”, “TNF signaling pathway”, and “NF-κB-mediated inflammatory response”, which are known to mediate acute mucosal inflammation and epithelial immune activation, highlighting their crucial roles in immune regulation during AGE. To further explore the mechanism by which active components of BXD act on these core targets, we selected 7-Methoxy-2-methyl-isoflavone and isorhamnetin—both highly ranked in the topology analysis with broad target coverage—for molecular docking and MD simulations with STAT3 and TNF, respectively.

Unlike most previous studies on BXD that focused on chronic gastric lesions or nonspecific inflammation, this study provides a disease-focused investigation of its molecular mechanism in AGE, a condition characterized by rapid epithelial injury, cytokine storm, and barrier dysfunction. By combining AGE-specific target datasets (GeneCards, OMIM, CTD) with molecular validation, this research uniquely identifies the TNF–STAT3 axis as a mechanistic hallmark of BXD's anti-AGE action. Such context-specific elucidation adds translational significance beyond conventional network pharmacology findings.

Simulation results demonstrated that these compounds formed stable complexes with the targets and exhibited favorable binding energies, corresponding to biologically plausible ligand–receptor interactions. This suggests that both molecules could interfere with the hyperactivated inflammatory signaling cascade characteristic of AGE and contribute synergistically to restoring epithelial immune balance.

GO and KEGG enrichment analyses revealed that the intersecting targets were significantly enriched in immune and inflammatory pathways such as "cytokine-cytokine receptor interaction", "IL-17 signaling pathway", and "T cell receptor signaling pathway", which are functionally linked to epithelial immune responses mediated by STAT3 and TNF (36, 37). Specifically, the IL-17 pathway promotes the expression of pro-inflammatory cytokines through STAT3 activation, while the TNF axis induces the production of downstream inflammatory cytokines, chemokines, and adhesion molecules, jointly driving epithelial infiltration and mucosal injury in AGE (12). Notably, our analysis also highlighted AGE-specific enrichment of epithelial integrity-related pathways such as "tight junction regulation" and "intestinal immune network for IgA production", suggesting that BXD may restore gut barrier homeostasis through multi-target modulation.

It should be acknowledged that enrichment analyses tend to prioritize broadly annotated immune and inflammatory pathways, which can lead to overrepresentation of common signaling cascades. Therefore, while the GO/KEGG results support a general anti-inflammatory role for BXD, we prioritized the TNF–STAT3 axis for deeper computational validation because (i) it consistently ranked highly across multiple topological metrics, (ii) it showed favorable docking and MM-PBSA energetics, and

(iii) it has direct mechanistic relevance to mucosal barrier dysfunction in gastroenteritis. We thus interpret pathway enrichment as hypothesis-generating and emphasize that the TNF–STAT3 axis represents a focused, testable mechanistic hypothesis for subsequent experimental validation.

STAT3 is a core factor in intracellular signal transduction and transcriptional activation, playing a key role in mucosal immune responses and inflammatory processes in the gastrointestinal tract. Numerous studies have shown that STAT3 can be activated by various inflammatory cytokines such as IL-6 and TNF-α, which subsequently triggers transcription of downstream genes, inducing inflammatory mediators and anti-apoptotic gene expression, contributing to intestinal barrier disruption and chronic inflammation maintenance (38, 39). Ogata et al. further demonstrated that IL-6 and TNF-α synergistically activate STAT3 signaling to regulate epithelial regeneration and inflammatory balance in intestinal tissues, emphasizing the crosstalk between these cytokines in acute mucosal (40). Such evidence supports our computational prediction that BXD may exert protective effects by disrupting the pathological feedback loop between TNF and STAT3 activation in AGE.

TNF-α is a typical pro-inflammatory cytokine that activates NF-κB and MAPK signaling pathways to induce the production of a large number of inflammatory mediators, serving as a major initiator of inflammation in AGE. Studies have reported that TNF-α is highly expressed in viral or bacterial gastroenteritis, and its antagonist, Infliximab, has been widely used in the treatment of IBD and other diseases (41). Together, these findings indicate that the TNF–STAT3 signaling axis may represent an essential pathological hub of acute intestinal inflammation and a principal target for BXD's multi-component therapeutic actions.

In our molecular docking and dynamics simulations, Isorhamnetin showed a binding energy of -8.4 kcal/mol with TNF. Docking visualization revealed that it could form multiple stable hydrogen bonds with TNF, maintaining a favorable binding state, suggesting its potential role in suppressing TNF-mediated inflammatory pathways. The active compound 7-Methoxy-2-methyl-isoflavone exhibited a binding energy of -8.7 kcal/mol with STAT3, and throughout the 100 ns simulation, its complex with STAT3 maintained stable RMSD values and persistent hydrogen bonds, with a calculated

binding free energy of -119.77 kJ/mol, indicating significant binding stability and pharmacological activity. Such high-affinity and stable interactions reinforce the hypothesis that these flavonoids could modulate intracellular inflammatory cascades through direct engagement with signal transducer proteins. In addition, previous studies have reported that flavonoids such as baicalein and quercetin can inhibit intestinal epithelial inflammation via the JAK2/STAT3 pathway (42), which is consistent with the mechanistic pattern observed in this study and further substantiates the predicted synergistic action among structurally related components of BXD.

Molecular dynamics simulations and MM-PBSA free energy decomposition further confirmed the binding stability and thermodynamic favorability of the core target–ligand complexes. Structural comparisons at different simulation time points (0, 25, 50, 75, and 100 ns) showed that all four complexes exhibited stable binding modes, concentrated energy distributions, and distinct free energy basins, suggesting sustained activity in physiological environments (22, 23, 30). Residue-wise energy decomposition also indicated that hydrophobic contacts and electrostatic stabilization jointly contributed to complex stability, particularly at the interface regions involving ILE-189, TYR-27 (STAT3), and PHE-109 (TNF).

In conclusion, BXD may exert multi-target therapeutic effects, including anti-inflammatory and mucosal-protective activities, through the synergistic modulation of STAT3 and TNF signaling pathways. This not only provides a solid structural and theoretical basis for the anti-AGE mechanism of BXD, but also demonstrates the great potential of integrating modern multi-technique strategies in traditional Chinese medicine formula research. Although in vitro or in vivo validation would further confirm these findings, the present study employs rigorous 100-ns MD simulations and thermodynamic calculations to ensure the reliability of the predicted interactions, offering a high-confidence foundation for future exploration. Planned future work includes targeted cell-based assays (e.g., LPS- or pathogen-stimulated Caco-2/HT-29 models to measure TNF, p-STAT3, and tight-junction proteins by Western blot/qPCR/TEER) and simplified AGE animal models to test efficacy and mechanism, as well as pharmacokinetic profiling to address flavonoid solubility and bioavailability. These steps will be essential to translate the computational predictions into

experimentally validated mechanistic insights.

References

1. Guarino A, Aguilar J, Berkley J, Broekaert I, Vazquez-Frias R, Holtz L, et al. Acute Gastroenteritis in Children of the World: What Needs to Be Done? J Pediatr Gastroenterol Nutr. 2020;70(5):694-701.
2. Freedman SB, Ali S, Oleszczuk M, Gouin S, Hartling L. Treatment of acute gastroenteritis in children: an overview of systematic reviews of interventions commonly used in developed countries. Evid Based Child Health. 2013;8(4):1123-37.
3. King CK, Glass R, Bresee JS, Duggan C, Centers for Disease C, Prevention. Managing acute gastroenteritis among children: oral rehydration, maintenance, and nutritional therapy. MMWR Recomm Rep. 2003;52(RR-16):1-16.
4. Zhuang Z, Wen J, Zhang L, Zhang M, Zhong X, Chen H, et al. Can network pharmacology identify the anti-virus and anti-inflammatory activities of Shuanghuanglian oral liquid used in Chinese medicine for respiratory tract infection? 2020;37:101139.
5. Ahmed SM, Hall AJ, Robinson AE, Verhoef L, Premkumar P, Parashar UD, et al. Global prevalence of norovirus in cases of gastroenteritis: a systematic review and meta-analysis. Lancet Infect Dis. 2014;14(8):725-30.
6. Zhou Z, An R, You L, Liang K, Wang X. Banxia Xiexin decoction: A review on phytochemical, pharmacological, clinical and pharmacokinetic investigations. Medicine (Baltimore). 2023;102(35):e34891.
7. Gong B, Xu Z, Wang Y, Feng Z, Li Z, Yu G, et al. Efficacy and safety of Banxia Xiexin Decoction in the treatment of gastric ulcer: A systematic review and meta-analysis of twenty-seven randomized controlled trials. 2023;5(9).
8. Zhang R, Zhu X, Bai H, Ning K. Network Pharmacology Databases for Traditional Chinese Medicine: Review and Assessment. Front Pharmacol. 2019;10:123.
9. Li S, Zhang B. Traditional Chinese medicine network pharmacology: theory, methodology and application. Chin J Nat Med. 2013;11(2):110-20.
10. Yu JG, Fan BS, Guo JM, Shen YJ, Hu YY, Liu X. Anisodamine Ameliorates Hyperkalemia during Crush Syndrome through Estradiol-Induced Enhancement of Insulin Sensitivity. Front Pharmacol. 2019;10:1444.
11. Wu X, Xu LY, Li EM, Dong GJCb, design d. Application of molecular dynamics simulation in biomedicine. 2022;99(5):789-800.
12. Yan S, Yue Y, Wang J, Li W, Sun M, Zeng L, et al. Banxia Xiexin decoction, a traditional Chinese medicine, alleviates colon cancer in nude mice. 2019;7(16):375.
13. He C, Zhou J, Zhang W, Zhang T, Pu YJJoE. Study on the bioactive components of Banxia Xiexin Decoction with different decocting methods and its effects on ulcerative colitis rats from the perspective of phase states. 2024;335:118626.
14. Wang W-L, Chen YJG. Network Pharmacology Prediction and Molecular Docking-Based Strategy to Explore the Potential Mechanism of Gualou Xiebai Banxia Decoction against Myocardial Infarction. 2024;15(4):392.
15. Ru J, Li P, Wang J, Zhou W, Li B, Huang C, et al. TCMSP: a database of systems pharmacology for drug discovery from herbal medicines. Journal of Cheminformatics. 2014;6(1):13.
16. Ge W, Fazal Z, Jakobsson EJFiAM, Statistics. Using optimal f-measure and random resampling in gene ontology enrichment calculations. 2019;5:20.

17. Meng XY, Zhang HX, Mezei M, Cui M. Molecular docking: a powerful approach for structure-based drug discovery. Current computer-aided drug design. 2011;7(2):146-57.
18. Hollingsworth SA, Dror ROJN. Molecular dynamics simulation for all. 2018;99(6):1129-43.
19. Lindorff-Larsen K, Piana S, Palmo K, Maragakis P, Klepeis JL, Dror RO, et al. Improved side-chain torsion potentials for the Amber ff99SB protein force field. Proteins. 2010;78(8):1950-8.
20. Sargolzaei M. Effect of nelfinavir stereoisomers on coronavirus main protease: Molecular docking, molecular dynamics simulation and MM/GBSA study. J Mol Graph Model. 2021;103:107803.
21. Kalin S, Comert Onder FJJoBS, Dynamics. Discovery of potential RSK1 inhibitors for cancer therapy using virtual screening, molecular docking, molecular dynamics simulation, and MM/GBSA calculations. 2025;43(3):1424-44.
22. Abraham MJ, Murtola T, Schulz R, Páll S, Smith JC, Hess B, et al. GROMACS: High performance molecular simulations through multi-level parallelism from laptops to supercomputers. 2015;1:19-25.
23. Genheden S, Ryde UJEoodd. The MM/PBSA and MM/GBSA methods to estimate ligand-binding affinities. 2015;10(5):449-61.
24. Wang C, Greene D, Xiao L, Qi R, Luo R. Recent Developments and Applications of the MMPBSA Method. Front Mol Biosci. 2017;4:87.
25. Dou W, Zhang J, Li H, Kortagere S, Sun K, Ding L, et al. Plant flavonol isorhamnetin attenuates chemically induced inflammatory bowel disease via a PXR-dependent pathway. The Journal of nutritional biochemistry. 2014;25(9):923-33.
26. Kim HR, Park CG, Jung JY. Acacetin (5,7-dihydroxy-4'-methoxyflavone) exhibits in vitro and in vivo anticancer activity through the suppression of NF-κB/Akt signaling in prostate cancer cells. International journal of molecular medicine. 2014;33(2):317-24.
27. Fang Y, Xiang W, Cui J, Jiao B, Su X. Anti-Inflammatory Properties of the Citrus Flavonoid Diosmetin: An Updated Review of Experimental Models. Molecules (Basel, Switzerland). 2024;29(7).
28. Chen Z, He Y, Hu F, Li M, Yao Y. Genkwanin Alleviates Mitochondrial Dysfunction and Oxidative Stress in a Murine Model of Experimental Colitis: The Participation of Sirt1. Annals of clinical and laboratory science. 2022;52(2):301-13.
29. Guo S, Wu X, Zheng J, Song M, Dong P, Xiao H. Anti-Inflammatory Property of 5-Demethylnobiletin (5-Hydroxy-6, 7, 8, 3', 4'-pentamethoxyflavone) and Its Metabolites in Lipopolysaccharide (LPS)-Induced RAW 264.7 Cells. Biology. 2022;11(12).
30. Meng X-Y, Zhang H-X, Mezei M, Cui MJCc-add. Molecular docking: a powerful approach for structure-based drug discovery. 2011;7(2):146-57.
31. Trott O, Olson AJ. AutoDock Vina: improving the speed and accuracy of docking with a new scoring function, efficient optimization, and multithreading. J Comput Chem. 2010;31(2):455-61.
32. Xu L, Zhang J, Wang Y, Zhang Z, Wang F, Tang XJBR. Uncovering the mechanism of Ge-Gen-Qin-Lian decoction for treating ulcerative colitis based on network pharmacology and molecular docking verification. 2021;41(2):BSR20203565.
33. Jiao X, Jin X, Ma Y, Yang Y, Li J, Liang L, et al. A comprehensive application: Molecular docking and network pharmacology for the prediction of bioactive constituents and elucidation of mechanisms of action in component-based Chinese medicine. 2021;90:107402.
34. Zhang W, Zhou Q, Chen X, Zhao J, Shi J, Chen LJAoM, et al. Exploring potential pharmacological mechanisms of Yiqi Tuomin Decoction in the treatment of allergic rhinitis utilizing

network pharmacology prediction and molecular docking-based strategies: experimental research. 2023;85(6):2662-76.
35. Jin Y, Yin X, Li Z, Xu JJAoPM. Mechanism of Baihe Decoction in the treatment of coronary heart disease based on network pharmacology and molecular docking. 2021;10(3):3205218-3218.
36. Gaffen SL, Jain R, Garg AV, Cua DJJNrI. IL-23-IL-17 immune axis: discovery, mechanistic understanding, and clinical testing. 2014;14(9):585.
37. Zhou Z, An R, You L, Liang K, Wang XJM. Banxia Xiexin decoction: A review on phytochemical, pharmacological, clinical and pharmacokinetic investigations. 2023;102(35):e34891.
38. Yu H, Pardoll D, Jove R. STATs in cancer inflammation and immunity: a leading role for STAT3. Nat Rev Cancer. 2009;9(11):798-809.
39. Grivennikov SI, Karin MJC, reviews gf. Dangerous liaisons: STAT3 and NF-κB collaboration and crosstalk in cancer. 2010;21(1):11-9.
40. Uno JK, Kolek OI, Hines ER, Xu H, Timmermann BN, Kiela PR, et al. The role of tumor necrosis factor alpha in down-regulation of osteoblast Phex gene expression in experimental murine colitis. Gastroenterology. 2006;131(2):497-509.
41. Atreya R, Neurath MFJVm. Current and future targets for mucosal healing in inflammatory bowel disease. 2017;33(1):82-8.
42. Xu J, Liu J, Yue G, Sun M, Li J, Xiu X, et al. Therapeutic effect of the natural compounds baicalein and baicalin on autoimmune diseases. 2018;18(1):1149-54.

Corresponding author email: 002161@hnucm.edu.cn

Funding

Postgraduate Scientific Research Innovation Project of Hunan Province, 20230830

Key Joint Project of National Natural Science Foundation of China, U22A20377

Approval of Graduate Research Innovation Projects at Hunan University of Chinese Medicine, 2025CX092

Competing Interests

The authors declare no competing interests.

Supplementary Files

This is a list of supplementary files associated with this preprint. Click to download.

- Checklist.docx
- Highlights.docx
- STAT37Methoxy2methylisoflavone90100ns.mp4